

Electroexcitation of nucleon resonances of the $[70, 1^-]$ multiplet in a light-front relativistic quark model

I.G. Aznauryan^{1,2} and V.D. Burkert¹

¹ Thomas Jefferson National Accelerator Facility, Newport News, Virginia 23606, USA

² Yerevan Physics Institute, 375036 Yerevan, Armenia

We utilize a light-front relativistic quark model to predict the $3q$ core contribution to the electroexcitation of nucleon resonances of the $[70, 1^-]$ multiplet on the proton and neutron at $Q^2 < 5 \text{ GeV}^2$. The investigation is stimulated in large degree by expected progress in the studies of the electroexcitation of nucleon resonances in the third resonance region in the CLAS experiment. For the resonances $N(1520)\frac{3}{2}^-$, $N(1535)\frac{1}{2}^-$, and $N(1675)\frac{5}{2}^-$, experimental data on electroexcitation amplitudes on the proton are available in a wide range of Q^2 . This allowed us to quantify the expected meson-baryon contributions to these amplitudes as a function of Q^2 .

PACS numbers: 12.39.Ki, 13.40.Gp, 14.20.Gk

I. INTRODUCTION

Experiments on the new generation of electron beam facilities CEBAF(Jefferson Lab), MAMI(Mainz), and MIT-Bates led to dramatic progress in the investigation of the electroexcitation of nucleon resonances, and significant role in the interpretation of new data belongs to quark models, in particular, to light-front relativistic quark models (LF RQM). The CLAS measurements at Jefferson Lab made possible, for the first time, the determination of the electroexcitation amplitudes of the Roper resonance $N(1440)\frac{1}{2}^+$ on the proton in a wide range of photon virtuality up to $Q^2 = 4.5 \text{ GeV}^2$ [1]. The comparison of these results with the LF RQM predictions [2, 3] was crucial for identification of the $N(1440)\frac{1}{2}^+$ as a predominantly radial excitation of a three-quark ($3q$) ground state, with additional non-3-quark contributions needed to describe the low Q^2 behavior of the amplitudes. The $\gamma^*p \rightarrow \Delta(1232)\frac{3}{2}^+$ transition amplitudes have been measured in a more wide range of Q^2 ($0.06 \div 8 \text{ GeV}^2$) [1, 4–10]. The obtained data strongly confirm the meson-cloud contribution as a source of the long-standing discrepancy between the data and quark model predictions for the magnetic-dipole form factor of this transition, and the 'bare' contribution to this form factor, obtained within dynamical reaction model [11–13] is very close to the LF RQM predictions [14–16]. Above 2 GeV^2 , the LF RQM [15] reproduces observed in experiment smallness of the ratio R_{EM} , as well the negative sign and sharply growing absolute value of the ratio R_{SM} for the $\gamma^*p \rightarrow \Delta(1232)\frac{3}{2}^+$ transition. A very interesting conclusion was made from the results on the $\gamma^*p \rightarrow N(1675)\frac{5}{2}^-$ amplitudes extracted from CLAS data [17]. A special feature of the resonance $N(1675)\frac{5}{2}^-$ is the strong suppression of the transverse helicity amplitudes for its excitation through quark transition from the proton. This feature allowed one to draw conclusion regarding the dominant strength of the meson-baryon contribution to the $\gamma^*p \rightarrow N(1675)\frac{5}{2}^-$ transverse helicity

amplitudes [18] which is supported by the results of the dynamical coupled-channels approach [13].

Experiments on meson electroproduction on new electron beam facilities have been performed on the proton target and, in the whole, allowed extraction of the electroexcitation amplitudes for the resonances $\Delta(1232)\frac{3}{2}^+$ [1, 4–10] and $N(1535)\frac{1}{2}^-$ [1, 19–22] in the range of Q^2 up to 8 GeV^2 , for the $N(1440)\frac{1}{2}^+$, $N(1520)\frac{3}{2}^-$, $N(1675)\frac{5}{2}^-$, $N(1680)\frac{5}{2}^+$, and $N(1710)\frac{1}{2}^+$ at $Q^2 < 4.5 \text{ GeV}^2$ [1, 17, 23–25], and for the $\Delta(1620)\frac{1}{2}^-$, $N(1650)\frac{1}{2}^-$, $\Delta(1700)\frac{3}{2}^-$, and $N(1720)\frac{3}{2}^+$ at $Q^2 = 0.65 \div 1.3 \text{ GeV}^2$ [23–25]. Currently new data are in preparation by the CLAS collaboration for the $ep \rightarrow ep\pi^0$ process in the same kinematics region as the CLAS data in the $ep \rightarrow en\pi^+$ channel [17, 26]. The two-channel analysis will allow for the separation of all resonances in the third nucleon resonance region at $Q^2 < 4.5 \text{ GeV}^2$. Other processes, such as $en(p_s) \rightarrow ep\pi^-(p_s)$ on deuterium target and $ep \rightarrow ep\pi^+\pi^-$ are also in preparation.

Therefore, in the near future CLAS experiment will provide us with rich information on the electroexcitation of the nucleon resonances from the multiplet $[70, 1^-]$ at $Q^2 < 4.5 \text{ GeV}^2$, and our goal in the present investigation is to extend our previous results on the electroexcitation of the $N(1520)\frac{3}{2}^-$ and $N(1535)\frac{1}{2}^-$ within LF RQM [27] by comprehensive investigation of electroexcitation of all resonances assigned to the $[70, 1^-]$ -plet on the proton and neutron.

We use an approach based on the LF dynamics which presents the most suitable framework for describing the transitions between relativistic bound systems [28–30]. In early works by Berestetsky and Terent'ev [29], the approach was based on the construction of the generators of the Poincaré group in the LF. It was later formulated in the infinite momentum frame (IMF) [31, 32]. This allowed one to demonstrate more clearly that diagrams which violate impulse approximation, i.e. the diagrams containing vertices like $\gamma^* \rightarrow q\bar{q}$, do not contribute. The interpretation of results for the $\gamma^*N \rightarrow N(N^*)$ transi-

tions in terms of the vertices $N(N^*) \leftrightarrow 3q$ and corresponding wave functions became more evident. A similar approach was developed and used in the investigation of electroexcitation of nucleon resonances in Ref. [2] within LF Hamiltonian dynamics [33]. Both approaches use complete set of orthogonal wave functions that correspond to the classification of the nucleon and nucleon resonances within the group $SU(6) \times O(3)$ in the c.m.s. of constituent quarks. It was shown in Ref. [32] that the wave functions of the system of quarks in the IMF and in their c.m.s. are related through Melosh rotations of quark spin matrices [34]. The same result was obtained in Ref. [2] within LF Hamiltonian dynamics.

The paper is organized as follows. In Sec. II we present the LF RQM formalism to compute the $\gamma^*N \rightarrow N^*$ transition amplitudes. We specify the IMF where the LF RQM is built and the relations between the $\langle N^* | J_{em}^\mu | N \rangle$ matrix elements and the $N(N^*) \leftrightarrow 3q$ wave functions in this frame. Further, the relations between these matrix elements and the $\gamma^*N \rightarrow N^*$ form factors and transition helicity amplitudes are presented. In Sec. III we discuss the mixings of the states $N(1535)\frac{1}{2}^-$ and $N(1650)\frac{1}{2}^-$, and $N(1520)\frac{3}{2}^-$ and $N(1700)\frac{3}{2}^-$. We discuss and present the available information on the corresponding mixing angles. The results are presented in Sec. IV and further summarized and discussed in Sec. V.

II. THE $\gamma^*N \rightarrow N^*$ TRANSITION AMPLITUDES IN LF RQM

The $\gamma^*N \rightarrow N^*$ transition amplitudes have been evaluated within the approach of Ref. [32] where the LF RQM is formulated in the infinite momentum frame chosen in such a way, that the initial hadron moves along the z -axis with the momentum $P \rightarrow \infty$, the virtual photon momentum is $k^\mu = \left(\frac{M^2 - m^2 - \mathbf{Q}_\perp^2}{4P}, \mathbf{Q}_\perp, -\frac{M^2 - m^2 - \mathbf{Q}_\perp^2}{4P} \right)$, the final hadron momentum is $P' = P + k$, and $Q^2 \equiv -k^2 = \mathbf{Q}_\perp^2$; m and M are masses of the nucleon and resonance, respectively. In this frame, the matrix elements of the electromagnetic current for the $\gamma^*N \rightarrow N^*$ transition have the form:

$$\begin{aligned} & \langle N^*, S'_z | J_{em}^\mu | N, S_z \rangle |_{P \rightarrow \infty} \\ &= 3eQ_a \int \Psi'^+(\mathbf{p}'_a, \mathbf{p}'_b, \mathbf{p}'_c) \Gamma_a^\mu \Psi(\mathbf{p}_a, \mathbf{p}_b, \mathbf{p}_c) d\Gamma, \end{aligned} \quad (1)$$

where S_z and S'_z are the projections of the hadron spins on the z -direction. In Eq. (1), it is supposed that the photon interacts with quark a (the quarks in hadrons are denoted by a, b, c), Q_a is the charge of this quark in units of e ($e^2/4\pi = 1/137$); Ψ and Ψ' are wave functions in the vertices $N(N^*) \leftrightarrow 3q$; \mathbf{p}_i and \mathbf{p}'_i ($i = a, b, c$) are the quark momenta in IMF; $d\Gamma$ is the phase space volume; Γ_a^μ corresponds to the vertex of the quark interaction with

the photon:

$$x_a \Gamma_a^x = 2p_{ax} + Q_x + iQ_y \sigma_z^{(a)}, \quad (2)$$

$$x_a \Gamma_a^y = 2p_{ay} + Q_y - iQ_x \sigma_z^{(a)}, \quad (3)$$

$$\Gamma_a^0 = \Gamma_a^z = 2P, \quad (4)$$

where x_i ($i = a, b, c$) is the fraction of the initial hadron momentum carried by the quark:

$$\mathbf{p}_i = x_i \mathbf{P} + \mathbf{q}_{i\perp}, \quad \sum_i \mathbf{q}_{i\perp} = 0, \quad \sum_i x_i = 1. \quad (5)$$

The invariant mass of the system of initial quarks has the form:

$$M_0^2 = \left(\sum_i p_i \right)^2 = \sum_i \frac{\mathbf{q}_{i\perp}^2 + m_q^2}{x_i}, \quad (6)$$

m_q is the quark mass.

Now we define the c.m.s. of initial quarks with the quark three-momenta \mathbf{q}_i ($i = a, b, c$), where quark transverse momenta are given by Eqs. (5), and the z -components are defined as:

$$q_{iz} + \omega_i = M_0 x_i, \quad \omega_i = \sqrt{m_q^2 + \mathbf{q}_i^2}, \quad (7)$$

$$q_{iz} = \frac{1}{2} \left(x_i M_0 - \frac{m_q^2 + \mathbf{q}_{i\perp}^2}{x_i M_0} \right), \quad (8)$$

$$M_0 = \sum_i \omega_i, \quad \sum_i \mathbf{q}_i = 0. \quad (9)$$

For the final state quarks, the quantities defined by Eqs. (5-9) are expressed through \mathbf{P}' , \mathbf{p}'_i , \mathbf{q}'_i , and M'_0 .

According to results of Ref. [32], the wave function Ψ in Eq. (1) is related to the wave function in the c.m.s. of quarks defined according to Eqs. (5-9) through Melosh matrices [34]:

$$\Psi = U^+(\mathbf{p}_a) U^+(\mathbf{p}_b) U^+(\mathbf{p}_c) \Psi_{fss} \Phi(\mathbf{q}_a, \mathbf{q}_b, \mathbf{q}_c). \quad (10)$$

Here we have separated the flavor-spin-space (Ψ_{fss}) and spatial (Φ) parts of the c.m.s. wave function. The Melosh matrices are

$$U(\mathbf{p}_i) = \frac{m_q + M_0 x_i + i\epsilon_{lm} \sigma_l q_{im}}{\sqrt{(m_q + M_0 x_i)^2 + \mathbf{q}_{i\perp}^2}}. \quad (11)$$

We construct the flavor-spin-space parts of the wave functions in the c.m.s. of quarks by utilizing the rules [2, 35] that correspond to the classification of the nucleon and nucleon resonances within the group $SU(6) \times O(3)$.

The phase space volume in Eq. (1) has the form:

$$d\Gamma = \frac{1}{(2\pi)^6} \frac{d\mathbf{q}_{b\perp} d\mathbf{q}_{c\perp} dx_b dx_c}{4x_a x_b x_c}. \quad (12)$$

A. The relations between matrix elements (1) and the $\gamma^* N \rightarrow N^*$ transition helicity amplitudes

Electroexcitation of the states with $J^P = \frac{1}{2}^-$ and $J^P = \frac{3}{2}^-, \frac{5}{2}^-$, that enter the multiplet $[70, 1^-]$, is described, respectively, by two and three form factors, which we define according to Refs. [36, 37] in the following way:

$$\langle N^*(\frac{1}{2}^-) | J_{em}^\mu | N \rangle \equiv e \bar{u}(P') \gamma_5 \tilde{J}^\mu u(P), \quad (13)$$

$$\langle N^*(\frac{3}{2}^-) | J_{em}^\mu | N \rangle \equiv e \bar{u}_\nu(P') \Gamma^{\nu\mu} u(P), \quad (14)$$

$$\langle N^*(\frac{5}{2}^-) | J_{em}^\mu | N \rangle \equiv e \bar{u}_{\nu\nu_1}(P') k^{\nu_1} \gamma_5 \Gamma^{\nu\mu} u(P), \quad (15)$$

where

$$\tilde{J}^\mu = (\not{k} k^\mu - k^2 \gamma^\mu) G_1 + [\not{k} \mathcal{P}^\mu - (\mathcal{P} k) \gamma^\mu] G_2, \quad (16)$$

$$\Gamma^{\nu\mu}(Q^2) = G_1 \mathcal{H}_1^{\nu\mu} + G_2 \mathcal{H}_2^{\nu\mu} + G_3 \mathcal{H}_3^{\nu\mu}, \quad (17)$$

$$\mathcal{H}_1^{\nu\mu} = \not{k} g^{\nu\mu} - k^\nu \gamma^\mu, \quad (18)$$

$$\mathcal{H}_2^{\nu\mu} = k^\nu P'^\mu - (k P') g^{\nu\mu}, \quad (19)$$

$$\mathcal{H}_3^{\nu\mu} = k^\nu k^\mu - k^2 g^{\nu\mu}, \quad (20)$$

$\mathcal{P} \equiv \frac{1}{2}(P' + P)$, $u(P), u(P')$ are the Dirac spinors, and $u_\nu(P'), u_{\nu\nu_1}(P')$ are the generalized Rarita-Schwinger spinors.

In the LF RQM under consideration, the form factors $G_i(Q^2)$ are derived through the matrix elements (1). For the $J^P = \frac{1}{2}^-$ resonances, the relations between form factors and the matrix elements (1) are following:

$$\frac{1}{2P} \langle N^*, \frac{1}{2} | J_{em}^{0,z} | N, \frac{1}{2} \rangle |_{P \rightarrow \infty} = Q^2 G_1(Q^2), \quad (21)$$

$$\begin{aligned} \frac{1}{2P} \langle N^*, \frac{1}{2} | J_{em}^{0,z} | N, -\frac{1}{2} \rangle |_{P \rightarrow \infty} = \\ = -\frac{M+m}{2} Q G_2(Q^2). \end{aligned} \quad (22)$$

For the $J^P = \frac{3}{2}^-$ resonances, these relations are following:

$$\begin{aligned} \frac{1}{2P} \langle N^*, \frac{3}{2} | J_{em}^{0,z} | N, \frac{1}{2} \rangle |_{P \rightarrow \infty} = \\ -\frac{Q}{\sqrt{2}} \left[G_1(Q^2) - \frac{M+m}{2} G_2(Q^2) \right], \end{aligned} \quad (23)$$

$$\frac{1}{2P} \langle N^*, \frac{3}{2} | J_{em}^{0,z} | N, -\frac{1}{2} \rangle |_{P \rightarrow \infty} = \frac{Q^2}{2\sqrt{2}} G_2(Q^2), \quad (24)$$

$$\langle N^*, \frac{3}{2} | J_{em}^x + i J_{em}^y | N, -\frac{1}{2} \rangle |_{P \rightarrow \infty} = \frac{Q^3}{\sqrt{2}} G_3(Q^2). \quad (25)$$

For the $J^P = \frac{5}{2}^-$ resonances, we have:

$$\begin{aligned} \frac{1}{2P} \langle N^*, \frac{5}{2} | J_{em}^{0,z} | N, \frac{1}{2} \rangle |_{P \rightarrow \infty} = \\ -Q^2 \left[G_1(Q^2) + \frac{M-m}{2} G_2(Q^2) \right], \end{aligned} \quad (26)$$

$$\frac{1}{2P} \langle N^*, \frac{5}{2} | J_{em}^{0,z} | N, -\frac{1}{2} \rangle |_{P \rightarrow \infty} = -\frac{Q^3}{2} G_2(Q^2), \quad (27)$$

$$\langle N^*, \frac{5}{2} | J_{em}^x + i J_{em}^y | N, -\frac{1}{2} \rangle |_{P \rightarrow \infty} = Q^4 G_3(Q^2). \quad (28)$$

The relations between the $\gamma^* N \rightarrow N^*$ helicity amplitudes and the form factors $G_1(Q^2), G_2(Q^2)$ are following:

$$A_{\frac{1}{2}} = b [2Q^2 G_1 - (M^2 - m^2) G_2], \quad (29)$$

$$S_{\frac{1}{2}} = -b \frac{K}{\sqrt{2}} \tilde{S}_{\frac{1}{2}}, \quad (30)$$

$$\tilde{S}_{\frac{1}{2}} = 2(M-m) G_1 + (M+m) G_2, \quad (31)$$

$$b \equiv e \sqrt{\frac{Q_+}{8m(M^2 - m^2)}}, \quad (32)$$

$$K \equiv \frac{\sqrt{Q_+ Q_-}}{2M}, \quad (33)$$

$$Q_\pm \equiv (M \pm m)^2 + Q^2. \quad (34)$$

For the resonances with $J^P = \frac{3}{2}^-$ and $\frac{5}{2}^-$ we have:

$$A_{1/2} = h_3 X, \quad A_{3/2} = \mp \sqrt{3} h_2 X, \quad (35)$$

$$S_{1/2} = \mp h_1 \frac{K}{\sqrt{2} M} X, \quad (36)$$

$$X \equiv K^{l-1} e \sqrt{\frac{Q_\pm}{32 J m (M^2 - m^2)}}, \quad l = J - \frac{1}{2}, \quad (37)$$

where

$$\begin{aligned} h_1(Q^2) = \mp 4M G_1(Q^2) + 4M^2 G_2(Q^2) + \\ 2(M^2 - m^2 - Q^2) G_3(Q^2), \end{aligned} \quad (38)$$

$$\begin{aligned} h_2(Q^2) = -2(\mp M + m) G_1(Q^2) - \\ (M^2 - m^2 - Q^2) G_2(Q^2) + 2Q^2 G_3(Q^2), \end{aligned} \quad (39)$$

$$\begin{aligned} h_3(Q^2) = \pm \frac{2}{M} [Q^2 + m(\mp M + m)] G_1(Q^2) + \\ (M^2 - m^2 - Q^2) G_2(Q^2) - 2Q^2 G_3(Q^2), \end{aligned} \quad (40)$$

and the upper and lower signs correspond, respectively, to $J^P = \frac{3}{2}^-$ and $\frac{5}{2}^-$ resonances.

III. MIXING OF $N(1535)\frac{1}{2}^-, N(1650)\frac{1}{2}^-$, AND $N(1520)\frac{3}{2}^-, N(1700)\frac{3}{2}^-$

The multiplet $[70, 1^-]$ consists of the following states: $N_{\frac{1}{2}}^{1-}(28_{1/2})$, $N_{\frac{3}{2}}^{3-}(28_{3/2})$, $N_{\frac{1}{2}}^{1-}(48_{1/2})$, $N_{\frac{3}{2}}^{3-}(48_{3/2})$,

$N_{\frac{1}{2}}^{5-}(^48_{5/2})$, $\Delta_{\frac{1}{2}}^{1-}(^210_{1/2})$, and $\Delta_{\frac{3}{2}}^{3-}(^210_{3/2})$, where we use the notation $^{2S+1}SU(3)_J$, which gives the assignment of the state according to the $SU(3)$ group, S is the total spin of the quarks, and J is the spin of the resonance. The resonances with $J^P = \frac{1}{2}^-$ and $\frac{3}{2}^-$ can be composed, respectively, from the states $^28_{1/2}$, $^48_{1/2}$ and $^28_{3/2}$, $^48_{3/2}$, and therefore can be mixings of these states:

$$N(1535)_{\frac{1}{2}}^{1-} = \cos\theta_S|^28_{1/2}\rangle - \sin\theta_S|^48_{1/2}\rangle, \quad (41)$$

$$N(1650)_{\frac{1}{2}}^{1-} = \sin\theta_S|^28_{1/2}\rangle + \cos\theta_S|^48_{1/2}\rangle, \quad (42)$$

$$N(1520)_{\frac{3}{2}}^{3-} = \cos\theta_D|^28_{3/2}\rangle - \sin\theta_D|^48_{3/2}\rangle, \quad (43)$$

$$N(1700)_{\frac{3}{2}}^{3-} = \sin\theta_D|^28_{3/2}\rangle + \cos\theta_D|^48_{3/2}\rangle. \quad (44)$$

There is information on the mixing angles θ_S and θ_D , obtained from the description of resonance masses within quark model with QCD-inspired interquark forces [38] and from experimental data on the decay widths of the resonances in the πN channel [39]. The results of Ref. [39] are based on the relations:

$$\langle \pi N | ^28_{1/2} \rangle / \langle \pi N | ^48_{1/2} \rangle = -2, \quad (45)$$

$$\langle \pi N | ^28_{3/2} \rangle / \langle \pi N | ^48_{3/2} \rangle = 2\sqrt{10}, \quad (46)$$

that follow from the $SU(6)_W$ -symmetry. The same relations have been obtained in Ref. [40] within the LF RQM by relating the $\langle \pi N | N^* \rangle$ amplitudes to the matrix elements of the axial-vector current $\langle N^* | J_{ax}^\mu | N \rangle$ using the hypothesis of partially conserved axial-vector current (PCAC) in the way suggested in Ref. [41]. The results of Ref. [39] are based on early data. Using recent data [43], we have revised the values of the mixing angles extracted from the πN widths of the resonances. As a result, we have obtained

$$\theta_S = -16.6 \pm 5^\circ, \quad \theta_D = 11.5 \pm 4^\circ, \quad (47)$$

instead of $\theta_S = -31.9^\circ$ and $\theta_D = 10.4^\circ$ in Ref. [39]. Large difference in θ_S is caused mainly by the significant change of the $N(1535)_{\frac{1}{2}}^{1-} \rightarrow \pi N$ width, that resulted in increasing of the ratio of the mean values of the $N(1535)_{\frac{1}{2}}^{1-}$ and $N(1650)_{\frac{1}{2}}^{1-} \pi N$ decay widths from 0.3 to 0.8.

The mixing angles obtained from the description of masses [38] are following:

$$\theta_S = -32^\circ, \quad \theta_D = 6.3^\circ. \quad (48)$$

IV. RESULTS

In this Section we present our results for the $3q$ core contribution to the helicity transition amplitudes for the electroexcitation of the resonances of the multiplet $[70, 1^-]$ on the proton and neutron (Figs. 1-12). The spacial part of the wave functions and parameters of the model have been specified in Ref. [27] via description of

the nucleon electromagnetic form factors by combining $3q$ and pion-cloud contributions in the LF dynamics. Good description of the nucleon electromagnetic form factors up to $Q^2 = 16 \text{ GeV}^2$ has been obtained with the nucleon wave function in the form:

$$|N\rangle = 0.95|3q\rangle + 0.313|\pi N\rangle, \quad (49)$$

and by employing two forms of the spatial wave function:

$$\Phi_1 \sim \exp(-M_0^2/6\alpha_1^2), \quad (50)$$

$$\Phi_2 \sim \exp[-(\mathbf{q}_a^2 + \mathbf{q}_b^2 + \mathbf{q}_c^2)/2\alpha_2^2], \quad (51)$$

with the following oscillator parameters and running quark masses:

$$\alpha_1 = 0.37 \text{ GeV}, \quad m_q^{(1)}(Q^2) = \frac{0.22 \text{ GeV}}{1 + Q^2/56 \text{ GeV}^2}, \quad (52)$$

$$\alpha_2 = 0.41 \text{ GeV}, \quad m_q^{(2)}(Q^2) = \frac{0.22 \text{ GeV}}{1 + Q^2/18 \text{ GeV}^2}. \quad (53)$$

For the resonances of the $[70, 1^-]$ -plet, the results for the transition amplitudes obtained with the wave functions (50,51) and corresponding parameters (52,53) are very close to each other. The role of running quark mass becomes visible above 3 GeV^2 . At $Q^2 = 5 \text{ GeV}^2$, it increases the transition helicity amplitudes by 25 – 35% and 10 – 15% for the wave functions (50) and (51), respectively.

Meson electroproduction gives strong evidence, that baryon resonances are not excited from quark transition alone, but there can be significant contribution from meson-baryon interaction, including pion-loop contributions generated by nearly massless pions. The common feature of all approaches that account for meson-baryon contributions is the fact that they are more rapidly losing their strength when Q^2 increases in comparison to the $3q$ contributions. For the $N(1535)_{\frac{1}{2}}^{1-}$ and $N(1520)_{\frac{3}{2}}^{3-}$, it is expected, that meson-baryon contributions can be neglected at $Q^2 > 2 \text{ GeV}^2$ [13]. There are accurate data for the electroexcitation of these resonances on the proton, respectively, at $Q^2 < 8$ and 4.5 GeV^2 . Therefore, the weight of the $3q$ contributions to the $N(1535)_{\frac{1}{2}}^{1-}$ and $N(1520)_{\frac{3}{2}}^{3-}$:

$$|N^*\rangle = c_{N^*}|3q\rangle + \dots, \quad c_{N^*} < 1, \quad (54)$$

we find from experimental values of the transition helicity amplitudes, assuming that at $Q^2 > 2 \text{ GeV}^2$ they are dominated by the $3q$ contributions. The weight factors c_{N^*} for the $N(1535)_{\frac{1}{2}}^{1-}$ and $N(1520)_{\frac{3}{2}}^{3-}$ are presented in the Captions to Figs. 1 and 6.

A. Mixings and the results for the $N(1535)_{\frac{1}{2}}^{1-}$, $N(1650)_{\frac{1}{2}}^{1-}$ and $N(1520)_{\frac{3}{2}}^{3-}$, $N(1700)_{\frac{3}{2}}^{3-}$

The results for the resonances $N(1535)_{\frac{1}{2}}^{1-}$, $N(1650)_{\frac{1}{2}}^{1-}$ and $N(1520)_{\frac{3}{2}}^{3-}$, $N(1700)_{\frac{3}{2}}^{3-}$ are shown in Figs. 1-4 and

6-9 taking into account mixings discussed in Section III. It can be seen, that the amplitudes for the resonances $N(1650)\frac{1}{2}^-$ and $N(1700)\frac{3}{2}^-$, taken as pure ${}^4\!8_{1/2}$ and ${}^4\!8_{3/2}$ states, are significantly smaller than the amplitudes for the $N(1535)\frac{1}{2}^-$ and $N(1520)\frac{3}{2}^-$. For this reason, the mixings play significant role in the electroexcitation of the $N(1650)\frac{1}{2}^-$ and $N(1700)\frac{3}{2}^-$, and in Figs. 3,4 and 8,9, we present three kind of curves: thin solid curves for the unmixed states ($\theta_S = \theta_D = 0$) and thick solid and dashed curves, respectively, for mixing angles from Eqs. (47) and (48). For the resonances $N(1535)\frac{1}{2}^-$ and $N(1520)\frac{3}{2}^-$, the corresponding curves are very close to each other.

It is known, that the results for the $\gamma^*N \rightarrow N^*$ transition amplitudes extracted from experimental data contain an additional sign related to the vertex of the resonance coupling to the final state hadrons (see, for example, Ref. [36]). In the electroproduction of pions on nucleons this is the relative sign between the πNN^* and πNN vertices. For the resonances of $[70, 1^-]$ -plet, this sign has been found in Ref. [40] in the LF approach based on PCAC (see also Section III). In Ref. [40], the electroexcitation of the resonances of $[70, 1^-]$ -plet on the proton and neutron has been investigated at $Q^2 = 0$, and the results for the transverse transition helicity amplitudes have been presented taking into account the relative sign between the πNN^* and πNN vertices. This sign is taken into account also in the results obtained in the present investigation and shown in Figs. 1-12. We mention, that from the relations (41,42,45) it follows that in all considered cases of mixings, the relative sign between the $\pi NN(1535)$ and $\pi NN(1650)$ vertices is negative. This is important for understanding of the results for the $N(1650)\frac{1}{2}^-$.

B. SQTm and the results for the $N(1675)\frac{1}{2}^-$

Now we comment on the results for the $N(1675)\frac{5}{2}^-$, Figs. 11,12. The approximation of the single quark transition model (SQTm) [42, 44–46] leads to selection rules, which for the resonances of the $[70, 1^-]$ -plet result in the suppression of the transition from the proton to the states with $S = \frac{3}{2}$ for the transverse helicity amplitudes. These are the states $N\frac{1}{2}^-({}^4\!8_{1/2})$, $N\frac{3}{2}^-({}^4\!8_{3/2})$, and $N\frac{5}{2}^-({}^4\!8_{5/2})$. According to our results, relativistic effects violate this suppression weakly. For the $J = \frac{1}{2}$ and $\frac{3}{2}$ states, this can be seen from Figs. 3, 8, where the amplitudes for the electroexcitation of $N\frac{1}{2}^-({}^4\!8_{1/2})$ and $N\frac{3}{2}^-({}^4\!8_{3/2})$ are given by the thin solid lines. For the resonance $N(1675)\frac{5}{2}^-$, we also have small violation of the suppression of the transverse helicity amplitudes for the electroexcitation on the proton (see Fig. 11). In contrast with proton, electroexcitation amplitudes on the neutron are large. In both cases, for proton and neutron,

close predictions have been obtained in the quark model of Ref. [47].

C. Inferred meson-baryon contributions

For the resonances $N(1520)\frac{3}{2}^-$, $N(1535)\frac{1}{2}^-$, and $N(1675)\frac{5}{2}^-$, experimental data on electroexcitation amplitudes on the proton are available in wide range of Q^2 . This allowed us to quantify the expected meson-baryon contributions to these amplitudes at $Q^2 < 2 - 3 \text{ GeV}^2$. The meson-baryon contributions inferred from the difference of the LF RQM predictions and the data are shown in Figs. 1, 6, 11 by thin dashed lines. They correspond approximately to the mean values of experimental data. The spread of these contributions can be deduced from the spread and errors of experimental data.

The constituent quark and inferred meson-baryon contributions can be associated, respectively, with the bare and meson-cloud contributions of the dynamical coupled-channels approaches that incorporate hadronic and electromagnetic channels. Much progress has been made recently within the EBAC/Argonne-Osaka coupled-channels analyses [13, 48, 49] that include pion photo- and electroproduction data. However, only preliminary results are available from the analyses that are based on the complete set of the CLAS pion electroproduction data in the whole Q^2 range up to 4.5 GeV^2 and from two channels $ep \rightarrow ep\pi^0$ and $ep \rightarrow en\pi^+$ [50, 51]. The results of the coupled-channels analyses are related to the resonance pole positions; with this in Refs. [13, 48] the absolute values of the meson cloud contributions continued to the real axis and evaluated at $W = 1.535, 1.52$, and 1.625 GeV , respectively, for the resonances $N(1520)\frac{3}{2}^-$, $N(1535)\frac{1}{2}^-$, and $N(1675)\frac{5}{2}^-$ are presented.

All inferred meson-baryon contributions have clear peak at $Q^2 = 0$, except the contributions for the $N(1520)\frac{3}{2}^- A_{1/2}(Q^2)$ amplitude and for the $N(1535)\frac{1}{2}^- S_{1/2}(Q^2)$ amplitude. Such pronounced peak is specific for the corresponding meson cloud contributions in the coupled-channels analyses [13, 48, 50, 51]. Concerning the $A_{1/2}(Q^2)$ amplitude for the $N(1520)\frac{3}{2}^-$, we mention that in all coupled-channels analyses [13, 48, 50, 51] the results for the meson cloud contribution are by order of magnitude and Q^2 dependence very close to our result.

For the states that are not affected by mixings, we present also in Table I the inferred meson-baryon contributions to the transverse transition helicity amplitudes at the photon point $Q^2 = 0$. According to our results, these contributions for the $N(1520)\frac{3}{2}^-$, $N(1535)\frac{1}{2}^-$, and $N(1675)\frac{5}{2}^-$ are dominated by the isovector component.

Resonance	proton				neutron			
	$A_{1/2}$	$A_{3/2}$	$A_{1/2}$	$A_{3/2}$	$A_{1/2}$	$A_{3/2}$	$A_{1/2}$	$A_{3/2}$
	exp. [43]		exp - LF RQM		exp. [43]		exp - LF RQM	
$N(1520)\frac{3}{2}^-$	-20 ± 5	140 ± 10	-17 ± 5	-174 ± 10	-50 ± 10	-115 ± 10	25 ± 10	131 ± 10
$N(1535)\frac{1}{2}^-$	115 ± 15		-54 ± 15		-75 ± 20		102 ± 20	
$\Delta(1620)\frac{1}{2}^-$	40 ± 15		-152 ± 15					
$N(1675)\frac{5}{2}^-$	19 ± 8	20 ± 5	16 ± 8	15 ± 5	-60 ± 5	-85 ± 10	-13 ± 5	-23 ± 10
$\Delta(1700)\frac{3}{2}^-$	140 ± 30	140 ± 30	-85 ± 30	-59 ± 30				

TABLE I: Transverse transition helicity amplitudes at $Q^2 = 0$ for several states of the $[70, 1^-]$ multiplet for proton and neutron (in units of $10^{-3} GeV^{-1/2}$). The first two columns show the RPP estimates [43]. Columns 3 and 4 show the inferred meson-baruon contributions obtained by subtraction the values obtained in the LF RQM from experimental data. The quoted uncertainties are from the experimental estimates.

V. SUMMARY AND DISCUSSION

In this paper we present the results of a comprehensive investigation of electroexcitation of nucleon resonances of the multiplet $[70, 1^-]$ on the proton and neutron within LF RQM. The investigation was stimulated by the expected progress in the extraction of the electroexcitation amplitudes for these resonances from the CLAS data, and also by the experiments on deuterium target.

It is known, that the three-quark structure of baryons resulted in predictions of a wealth of excited states with underlying spin-flavor and orbital symmetry of $SU(6) \times O(3)$. In spite of the essentially non-relativistic nature of this symmetry, it describes well the observed quantum numbers and in many cases masses of the resonances in the first, second, and third nucleon resonance regions. The LF dynamics is known as most suitable framework for describing transitions of baryons composed of relativistic constituent quarks. The important feature of the LF approach of Ref. [32], employed in the present investigation, as well of the LF approach of Ref. [2], is the fact that these approaches could solve in uniform way the problem of construction of orthogonal set of wave functions for the relativistic quarks by preserving the $SU(6) \times O(3)$ symmetry. This has been done by setting the $SU(6) \times O(3)$ symmetry in the c.m.s. of constituent quarks defined by Eqs. (5-9). Then it was shown, that in the IMF or LF framework, which are used for calculation of the transition amplitudes, the flavour-spin-space part of wave functions are related to the wave functions in c.m.s. of quarks by quark spin rotations given by the Melosh matrices. Therefore, in our calculations we employ the flavor-spin-space parts of the wave functions that in the c.m.s. of quarks correspond to the classification of

states within the group $SU(6) \times O(3)$.

The pairs of resonances $N(1535)\frac{1}{2}^-$, $N(1650)\frac{1}{2}^-$ and $N(1520)\frac{3}{2}^-$, $N(1700)\frac{3}{2}^-$ with the same spin-parity can be composed, respectively, from the states $^2 8_{1/2}$, $^4 8_{1/2}$ and $^2 8_{3/2}$, $^4 8_{3/2}$. Therefore, they can be mixings of these states. There is information on the mixing angles, obtained from the description of resonance masses within quark model with QCD-inspired interquark forces [38] and from experimental data on the decay widths of the resonances in the πN channel [39]. The results of Ref. [39] are based on the early data. Using recent data [43], we have revised the values of the mixing angles extracted from the πN widths of the resonances. In our calculations of the electroexcitation amplitudes for the $N(1535)\frac{1}{2}^-$, $N(1650)\frac{1}{2}^-$, $N(1520)\frac{3}{2}^-$, and $N(1700)\frac{3}{2}^-$ we have used two sets of mixing angles: obtained from the description of mass in Ref. [38] and found in the present work from the πN widths of the resonances. The calculated amplitudes for the electroexcitation of the states $^4 8_{1/2}$ and $^4 8_{3/2}$ turned out significantly smaller than the amplitudes for the states $^2 8_{1/2}$ and $^2 8_{3/2}$. As a result, the mixings do not affect practically the electroexcitation amplitudes for the $N(1535)\frac{1}{2}^-$ and $N(1520)\frac{3}{2}^-$, but play a significant role for the $N(1650)\frac{1}{2}^-$ and $N(1700)\frac{3}{2}^-$.

The approximation of the single quark transition model [42, 44–46] leads to selection rules, which for the resonance $N(1675)\frac{5}{2}^-$ result in the suppression of the amplitudes $A_{1/2}(Q^2)$ and $A_{3/2}(Q^2)$ on the proton. According to our results, relativistic effects violate this suppression weakly, and we expect that experimental values of these amplitudes will be determined mostly by the meson-baryon contributions. In contrast with proton, the predicted electroexcitation amplitudes on the neutron for

the $N(1675)\frac{5}{2}^-$ are large.

For the resonances $N(1520)\frac{3}{2}^-$, $N(1535)\frac{1}{2}^-$, and $N(1675)\frac{5}{2}^-$, experimental data on electroexcitation amplitudes on the proton are available in wide range of Q^2 . This allowed us to present the expected meson-baryon contributions to these amplitudes at $Q^2 < 2 - 3 \text{ GeV}^2$ inferred from the difference of the LF RQM predictions and the data. The correspondence between these contributions and the meson cloud contributions obtained

within the EBAC/Argonne-Osaka coupled-channels analyses [13, 48–51] is discussed in Sec. IV C.

Acknowledgments. This work was supported by the U.S. Department of Energy, Office of Science, Office of Nuclear Physics, under Contract No. DE-AC05-06OR23177, and the National Science Foundation, State Committee of Science of the Republic of Armenia, Grant No. 15T-1C223.

-
- [1] I. G. Aznauryan, et al., CLAS collaboration, Phys. Rev. C **80**, 055203 (2009).
 - [2] S. Capstick and B. D. Keister, Phys. Rev. D **51**, 3598 (1995).
 - [3] I. G. Aznauryan, Phys. Rev. C **76**, 025212 (2007).
 - [4] S. Stave et al., Eur. Phys. J. A **30**, 471 (2006); Phys. Rev. C **78**, 025209 (2008).
 - [5] N.F. Sparveris et al., Phys. Rev. Lett. **94**, 022003 (2005); Phys. Lett. B **651**, 102 (2007).
 - [6] C. Mertz et al., Phys. Rev. Lett. **86**, 2963 (2001).
 - [7] C. Kunz et al., Phys. Lett. B **564**, 21 (2003).
 - [8] V.V. Frolov et al., Phys. Rev. Lett. **82**, 45 (1999).
 - [9] A.N. Villano et al., Phys. Rev. C **80**, 035203 (2009).
 - [10] J. J. Kelly et al., Phys. Rev. Lett. **95**, 102001 (2005); Phys. Rev. C **75**, 025201 (2007).
 - [11] T. Sato and T.-S. H. Lee, Phys. Rev. C **63**, 055201 (2001).
 - [12] V. D. Burkert and T.-S. H. Lee, Int. J. Mod. Phys. E **13**, 1035 (2004).
 - [13] B. Juliá-Díaz, T.-S. H. Lee, A. Matsuyama, T. Sato, and L. C. Smith, Phys. Rev. C **77**, 045205 (2008).
 - [14] B. Juliá-Díaz, D. O. Riska, and F. Coester, Phys. Rev. C **69**, 035212 (2004).
 - [15] I. G. Aznauryan and V. D. Burkert, Phys. Rev. C **92**, 035211 (2015).
 - [16] I. G. Aznauryan and V. D. Burkert, arXiv:1603.06692, 2015.
 - [17] K. Park, et al., CLAS collaboration, Phys. Rev. C **91**, 045203 (2015).
 - [18] I. G. Aznauryan and V. D. Burkert, Phys. Rev. C **92**, 015203 (2015).
 - [19] R. Thompson et al., CLAS Collaboration, Phys. Rev. Lett. **86**, 1702 (2001).
 - [20] H. Denizli et al., CLAS Collaboration, Phys. Rev. C **76**, 015204 (2007).
 - [21] C.S. Armstrong et al., Phys. Rev. D **60**, 052004 (2009).
 - [22] M.M. Dalton et al., Phys. Rev. C **80**, 015205 (2009).
 - [23] V.I. Mokeev and I.G. Aznauryan, Int. J. of Modern Phys., Conf. Series, **26**, 1460080 (2014).
 - [24] V.I. Mokeev et al., arXiv:1509.05465[nucl-ex].
 - [25] V.I. Mokeev et al., CLAS Collaboration, Phys. Rev. C **86**, 035203 (2012).
 - [26] K. Park et al., CLAS Collaboration, Phys. Rev. C **77**, 015208 (2008).
 - [27] I. G. Aznauryan and V. D. Burkert, Phys. Rev. C **85**, 055202 (2012).
 - [28] S. D. Drell and T. M. Yan, Phys. Rev. Lett. **24**, 181 (1970).
 - [29] V. B. Berestetskii and M. V. Terent'ev, Sov. J. Nucl. Phys., **24**, 1044 (1976); **25**, 347 (1977).
 - [30] S. J. Brodsky and S. D. Drell, Phys. Rev. D **22**, 2236 (1980).
 - [31] L. A. Kondratyuk and M. V. Terent'ev, Yad. Fiz., **31**, 1087 (1980).
 - [32] I. G. Aznauryan, A. S. Bagdasaryan, and N. L. Ter-Isaakyan, Phys. Lett. B **112**, 393 (1982); Yad. Fiz. **36**, 1278 (1982).
 - [33] B. D. Keister and W. N. Polizou, Adv. Nucl. Phys. **20**, 225 (1991).
 - [34] H. J. Melosh, Phys. Rev. D **9**, 1095 (1974).
 - [35] R. Koniuk and N. Isgur, Phys. Rev. D **21**, 1868 (1980).
 - [36] I. G. Aznauryan, V. D. Burkert, Prog. Part. Nucl. Phys. **67**, 1 (2012), arXiv:1109.1720, 2011.
 - [37] R.C.E. Devenish, T.S. Eisenschitz, and J.G. Körner, Phys. Rev. D **14**, 3063 (1976).
 - [38] N. Isgur and G. Karl, Phys. Rev. D **18**, 4187 (1978).
 - [39] A. J. G. Hey, R. J. Litchfield, and R. J. Cashmore, Nucl. Phys. B **95**, 516 (1975).
 - [40] I. G. Aznauryan and A. S. Bagdasaryan, Yad. Fiz. **41**, 249 (1985).
 - [41] F. J. Gilman, M. Kugler, and S. Meshkov, Phys. Rev. D **9**, 715 (1974).
 - [42] A.J.G. Hey and J. Weyers, Phys. Lett. B **48**, 69 (1974).
 - [43] C. Patrignani et al. [Particle Data Group], Chinese Physics C **40**, 100001 (2016).
 - [44] J. Babcock and J.L. Rosner, Ann. Phys. (N.Y.) **96**, 191 (1976).
 - [45] W.N. Cottingham and I.H. Dunbar, Z. Phys. C **2**, 41 (1979).
 - [46] V.D. Burkert et al., Phys. Rev. C **67**, 035204 (2003).
 - [47] E. Santopinto and M. M. Giannini, Phys. Rev. C **86**, 065202 (2012).
 - [48] B. Juliá-Díaz, H. Kamano, T.-S. H. Lee, A. Matsuyama, T. Sato, and N. Suzuki, Phys. Rev. C **80**, 025207 (2009).
 - [49] H. Kamano, S. X. Nakamura, T.-S. H. Lee, and T. Sato, Phys. Rev. C **94**, 015201 (2016).
 - [50] H. Kamano, talk presented on INT workshop "Spectrum and Structure of Excited Nucleons from Exclusive Electroproduction", Seattle, USA, November, 2016.
 - [51] T. Sato, talk presented on INT workshop "Spectrum and Structure of Excited Nucleons from Exclusive Electroproduction", Seattle, USA, November, 2016.

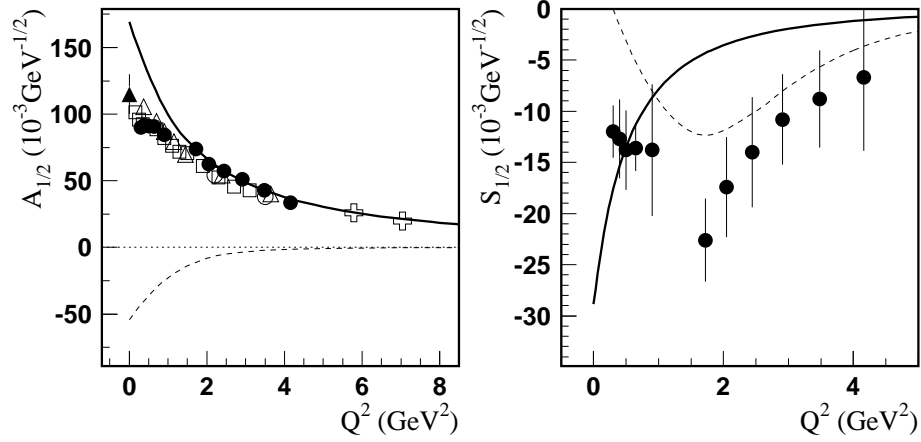


FIG. 1: The $\gamma^* p \rightarrow N(1535)\frac{1}{2}^-$ transition helicity amplitudes. The solid curves are the LF RQM predictions; the weight factors for the $3q$ contributions to the nucleon and resonance are taken into account according to Eqs. (49) and (54) with $c_{N^*} = 0.84$ and 0.94 for the mixing angles $\theta_S = -16.6^\circ$ and -32° , respectively, (see Eqs.(47) and (48)). The thin dashed curves present the inferred meson-baryon contributions (see Sec. IV C). Solid circles are the amplitudes extracted from CLAS pion electroproduction data [1]. The open triangles [19] and open boxes [20] are the amplitudes extracted from the JLab/Hall B η electroproduction data; the open circles [21] and open crosses [22] are the amplitudes extracted from the JLab/Hall C η electroproduction data; the full triangle at $Q^2 = 0$ is the RPP estimate [43].

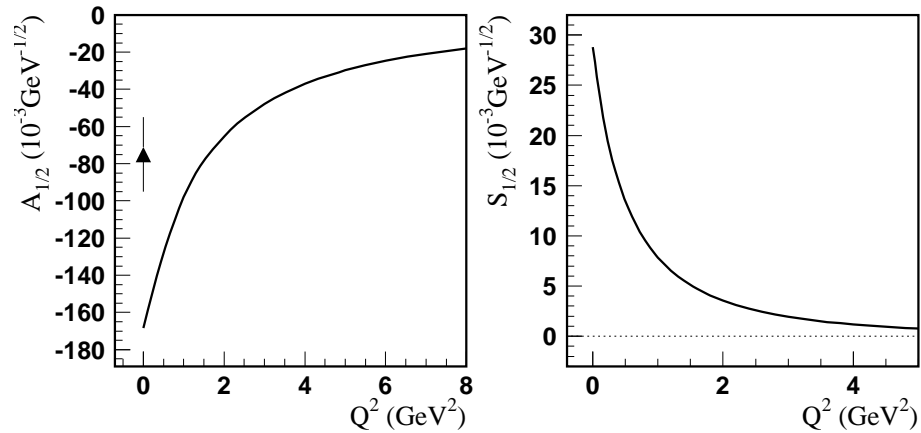


FIG. 2: The $\gamma^* n \rightarrow N(1535)\frac{1}{2}^-$ transition helicity amplitudes. Legend for the solid curves is as for Fig. 1. The full triangle at $Q^2 = 0$ is the RPP estimate [43].

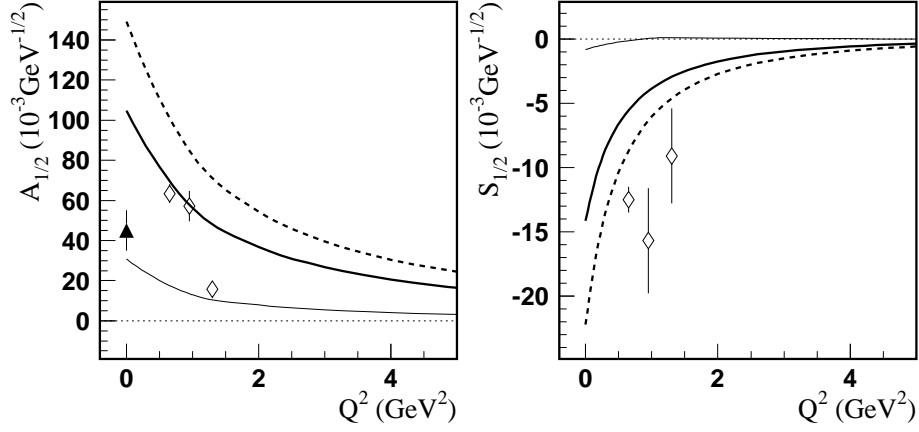


FIG. 3: The $\gamma^* p \rightarrow N(1650)\frac{1}{2}^-$ transition helicity amplitudes. The LF RQM predictions are shown by thin and thick solid lines for the mixing angles $\theta_S = 0$ and -16.6° , respectively, and by thick dashed lines for $\theta_S = -32^\circ$ (see Eqs.(47) and (48)). The full triangle at $Q^2 = 0$ is the RPP estimate [43]; open rhombuses are the amplitudes extracted from CLAS 2π electroproduction data [23].

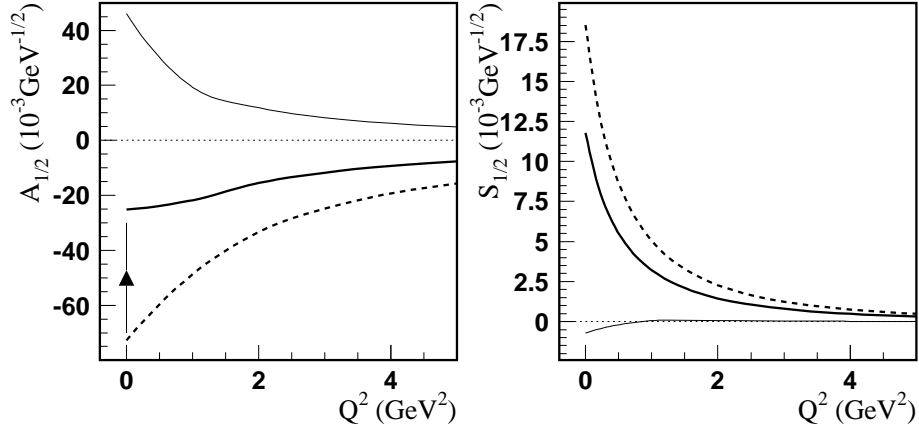


FIG. 4: The $\gamma^* n \rightarrow N(1650)\frac{1}{2}^-$ transition helicity amplitudes. Legend for the lines is as for Fig. 3. The full triangle at $Q^2 = 0$ is the RPP estimate [43].

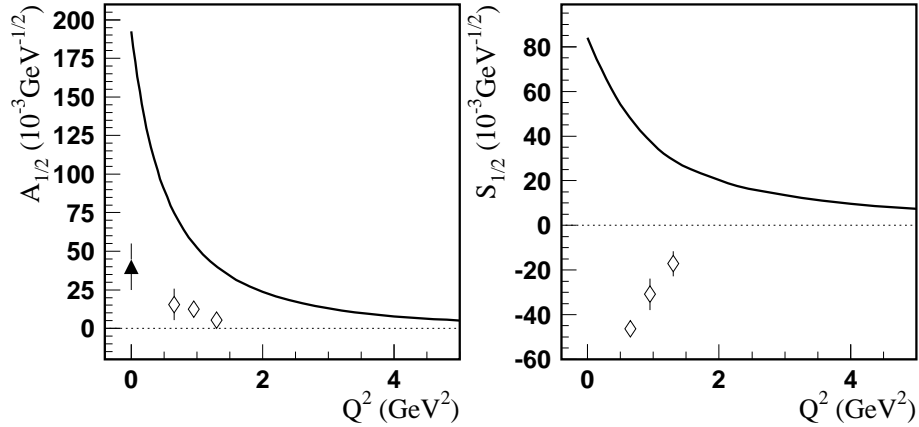


FIG. 5: The $\gamma^* p \rightarrow \Delta(1620)\frac{1}{2}^-$ transition helicity amplitudes. The solid curves are the LF RQM predictions. The full triangle at $Q^2 = 0$ is the RPP estimate [43]; open rhombuses are the amplitudes extracted from CLAS 2π electroproduction data [24].

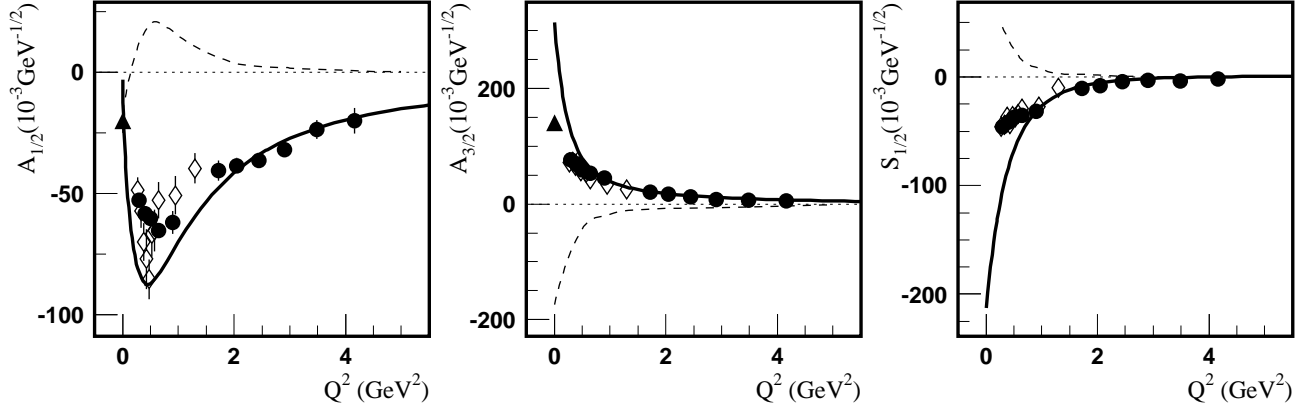


FIG. 6: The $\gamma^* p \rightarrow N(1520)_{\frac{3}{2}}^-$ transition helicity amplitudes. The solid curves are the LF RQM predictions; the weight factors for the $3q$ contributions to the nucleon and resonance are taken into account according to Eqs. (49) and (54) with $c_{N^*} = 0.92$ and 0.94 for the mixing angles $\theta_D = 6.3^\circ$ and 11.5° , respectively, (see Eqs.(47) and (48)). The thin dashed curves present the inferred meson-baryon contributions (see Sec. IV C). Solid circles are the amplitudes extracted from CLAS pion electroproduction data [1]; open rhombuses are the amplitudes extracted from CLAS 2π electroproduction data [23–25]. The full triangles at $Q^2 = 0$ are the RPP estimates [43].

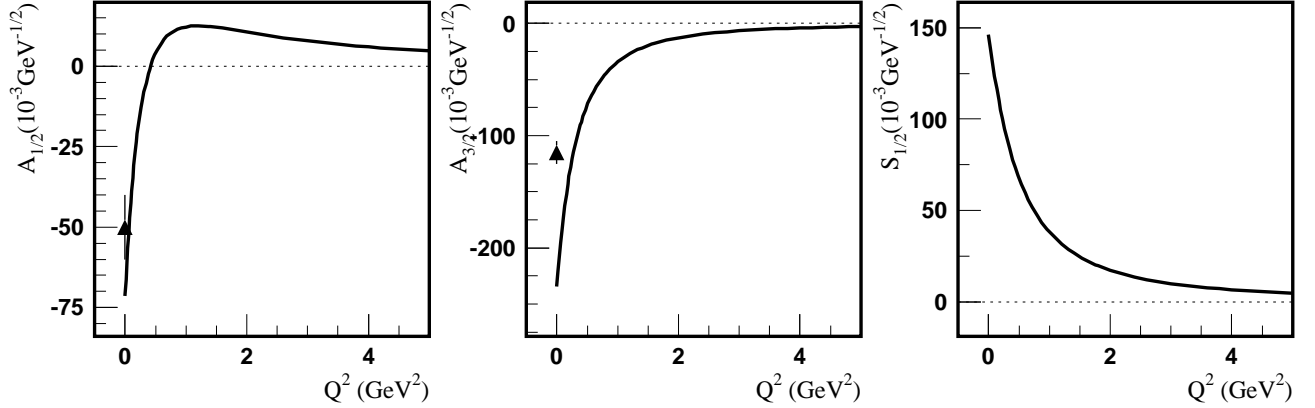


FIG. 7: The $\gamma^* n \rightarrow N(1520)_{\frac{3}{2}}^-$ transition helicity amplitudes. Legend for the solid curves is as for Fig. 6. The full triangles at $Q^2 = 0$ are the RPP estimate [43].

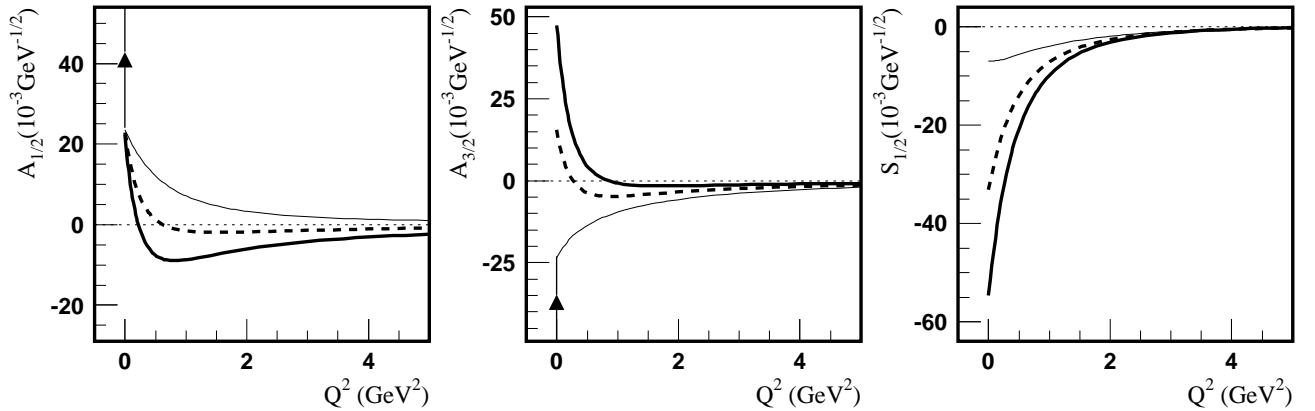


FIG. 8: The $\gamma^* p \rightarrow N(1700)_{\frac{3}{2}}^-$ transition helicity amplitudes. The LF RQM predictions are shown by the thin and thick solid lines for the mixing angles $\theta_S = 0$ and 11.5° , respectively, and by thick dashed lines for $\theta_S = 6.3^\circ$ (see Eqs.(47) and (48)). The full triangles at $Q^2 = 0$ are the RPP estimates [43].

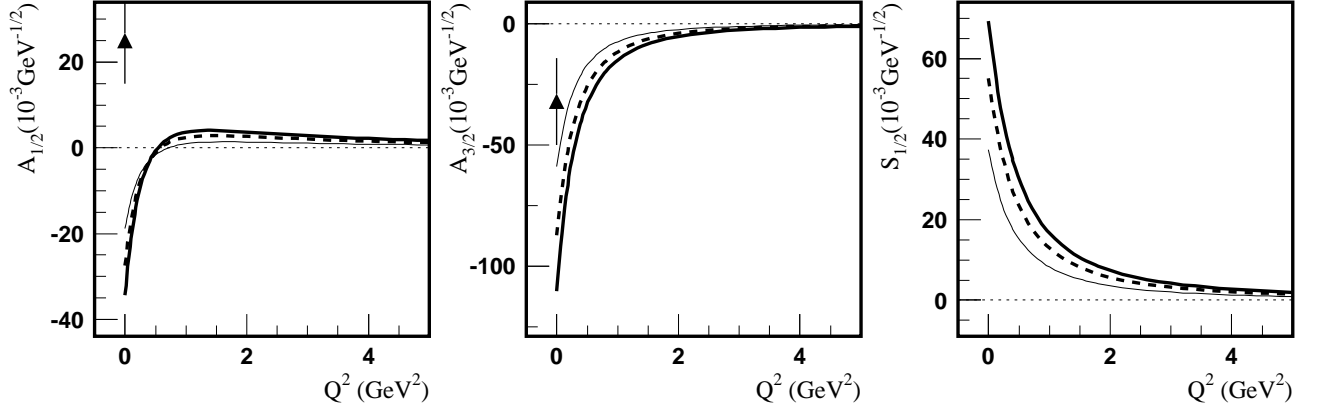


FIG. 9: The $\gamma^* n \rightarrow N(1700)_{\frac{3}{2}}^-$ transition helicity amplitudes. Legend for the lines and data is as for Fig. 8.

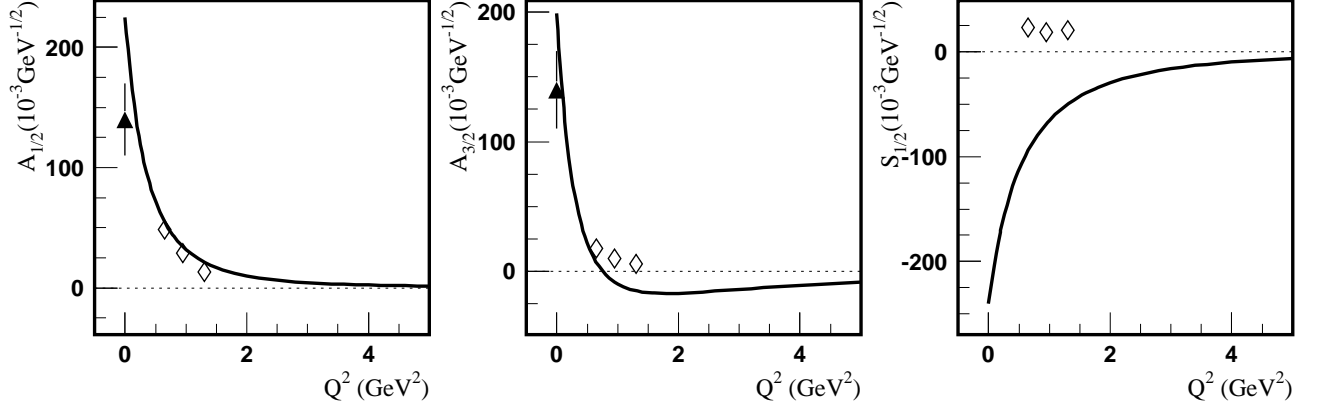


FIG. 10: The $\gamma^* p \rightarrow \Delta(1700)_{\frac{3}{2}}^-$ transition helicity amplitudes. The solid curves are the LF RQM predictions. The full triangles at $Q^2 = 0$ are the RPP estimates [43]; open rhombuses are the amplitudes extracted from CLAS 2π electroproduction data [23].

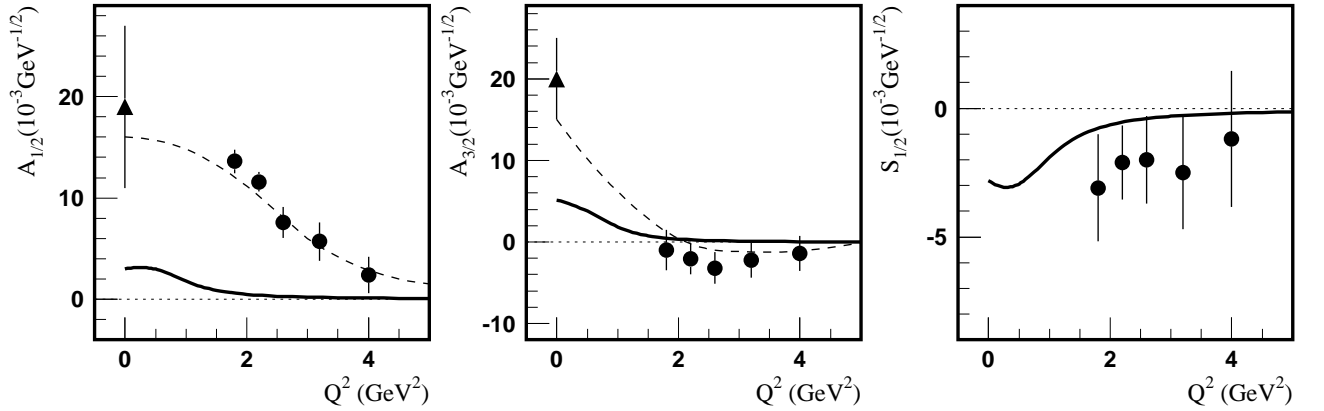


FIG. 11: The $\gamma^* p \rightarrow N(1675)_{\frac{5}{2}}^-$ transition helicity amplitudes. The solid curves are the LF RQM predictions. The thin dashed curves present the inferred meson-baryon contributions (see Sec. IV C). The full triangles at $Q^2 = 0$ are the RPP estimates [43]; the solid circles are the amplitudes extracted from CLAS π electroproduction data [17].

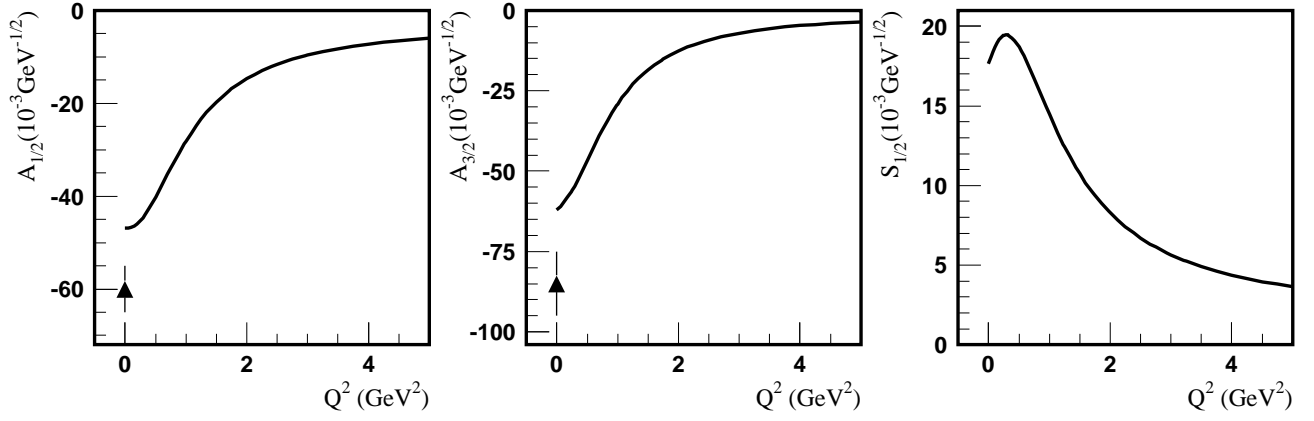


FIG. 12: The $\gamma^* n \rightarrow N(1675)_{\frac{5}{2}}^-$ transition helicity amplitudes. The solid curves are the LF RQM predictions. The full triangles at $Q^2 = 0$ are the RPP estimates [43].